COMPUTATIONAL MATERIALS SCIENCE GROUP

DEPARTMENT OF PHYSICS

RESEARCH AND SCHOLARLY ACTIVITIES

2013

Introduction

The Computational Materials Science Group (CMSG) focuses on problems dealing with modeling aspects that support experimental Solid State Physics, Materials Science, Genomics, Engineering, among other multidisciplinary scientific areas. Interested staff and students from University of Eldoret, other universities and tertiary institutions in Kenya and the region are invited to undertake collaborative work with us. We have several international collaborative links ensuring that our research themes produce high quality peer-reviewed international publications and have current relevance to community. This report presents highlights of some of the group activities in 2013. The group currently consists of the following members:

Staff Members

1. Nicholas W Makau, BSc (Moi) MSc (Moi) PhD (Witwatersrand, RSA, DAAD sponsored)
2. George O Amolo, BSc (Moi) Msc (Nairobi, DAAD sponsored) PhD (Witwatersrand, RSA, DAAD sponsored)
3. Joseph Z Mapelu, BSc (Moi) Msc (Nairobi, DAAD sponsored) PhD (Moi, DAAD sponsored)
4. Rogers Koech, BSc (Moi) (MSc candidate-JKUAT)–Computer Science- (System Administrator)

Current Postgraduate Students

1. Winfred Mulwa, BSc (Kampala) Msc (Eldoret) PhD candidate
2. Henry Otunga, BSc (Maseno) MSc (Maseno) (Dphil candidate - Maseno/Eldoret)
3. Phillip W O Nyawere, BSc (Kenyatta) MSc (Moi) PhD (Eldoret)
4. Dennis Magero, BSc (Moi) Msc (Eldoret) PhD candidate

5. Mike Atambo, BSc (Moi) MSc (Eldoret) (System Administrator)
6. Victor Meng'wa, BEd Sc (Egerton) (MSc candidate – Eldoret)
7. Patrick Mwonga, BEd Sc (Kenyatta) (MSc candidate – Eldoret)
8. Peter Kirui, BEd Sc (Egerton) (MSc candidate – Eldoret)
9. Felix Dusabirane, Bsc (Kigali) (MSc candidate – Eldoret)
10. Carolyne Bakasa, Bsc (Moi) (MSc candidate – Eldoret)

Latest Peer-Reviewed Publications

(see attached publications at the end of report)

Conferences Presentations/Schools Attended

Dennis Magero, Victor Meng'wa, Winfred Mulwa and Patrick Mwonga made conference presentations in the Materials Science and Solar Energy in East and Southern Africa (MSSEESA) held in Nairobi in November 2013. The works they presented are, respectively, *(1) The Hydrogen Economy – Materials for Hydrogen Storage Surface-Dennis Magero; (2) Calculations for (110) Surface Rutile TiO_2 and SnO_2 for Dye Sensitized Solar Cells-Victor Mengw'a* and *(3) First Principle Calculations of Nb:TiO_2 for Solar Cells Applications – Winfred Mulwa*. (4) Studies of Intrinsic defects in TiO2: A DFT Study – Patrick Mwonga.

George Amolo presented an invited talk, "*ab initio* studies of hard materials and materials for solar energy utilization", in the 7th African Materials Research Society (AMRS), held in Addis Ababa, 8 – 13th December 2013.

Victor Meng'wa and Winfred Mulwa made conference presentations in the 7th African Materials Research Society (AMRS), held in Addis Ababa, 8 – 13th December 2013: *Calculations for (110) Surface Rutile TiO_2 and SnO_2 for Dye Sensitized Solar Cells by Victor Mengw'a* and *First Principle Calculations of Nb:TiO_2 for Solar Cells Applications by Winfred Mulwa*.

Mike Atambo attended a QMC School in JAIST, Japan, from 19th – 23rd February 2013**.**

Graduations:

1. Mulwa, Winifred: graduated with an MSc on 3rd December 2013. She has already registered for a PhD at University of Eldoret.

2. Magero, Dennis: graduated with an MSc on 3rd December 2013 being the 1st student from a Chemistry/Physics collaboration in the group. He has made an application for a PhD sandwich Programme with Josef Fourier University in Grenoble, France, in a joint project with the Computational Materials Science Group, University of Eldoret, Kenya. From the French end is Professor Mark Casida, a world reknown Quantum Chemist. Professor Casida has visited our group twice. His initial visit was in the 2nd African School on Electronic Structure Methods and Applications (ASESMA 2012) held in Eldoret and partly sponsored by NCST funds. His second visit was partly sponsored by the French Embassy, Nairobi, and University of Eldoret in May 2013.

3. Atambo, Mike: graduated with an MSc on 3rd December 2013. He is likely to register for a PhD under a joint project with Professor Ryo Maezono of the Japan Advanced Institute of Science and Technology (JAIST). Professor Maezono and his colleagues has visited our group 3 times and his research associate, Dr Kenta Hongo, is expected to visit us on 22nd of February 2014. This collaboration with the Japanese group has resulted in the drafting of joint proposals, two of which have been submitted to the NCST/JSPS calls but so far with no success. This group has also been kind enough to donate computing infrastructure which now forms equipment for our research group in Eldoret and hence the university. A draft publication following the work of Mike Atambo and a Japanese student, Kentaro Hayashi, from JAIST, has been in preparation for several months now and is expected to be ready soon for submission to a journal.

4. Meng'wa, Victor: submitted his MSc thesis and is awaiting oral defence. The work of Victor has gotten interest from Prof Ralph Gebauer, a scientist in the International Centre for Theoretical Physics (ICTP), Trieste, Italy. There have been negotiations to get Victor to register for a PhD under the Sandwich Training Education Program (STEP), which will provide him with funding to visit ICTP to consult a supervisor in Italy for a period of up to 4 months per year for 3 years.

5. Nyawere, Philip: Graduated with a PhD on 3rd December 2013. He is a member of staff in Kabarak University. His work on defects in materials is related to the current work on devices to be fabricated. His thesis has produced 2 peer-reviewed international publications.

6. Rop Ronald: Graduated with a PhD on 3rd December 2013. He is a member of staff in Egerton University. His thesis has produced 2 peer-reviewed international publications.

7. Ronno, Cosmas: Graduated with a PhD on 3rd December 2013. He is a member of staff in University of Eldoret. His work on Solar Energy Radiation is related to the current work on devices to be fabricated. He is currently working on a number of publications.

Research/Training Visits

2013

1. Nicholas Makau and George Amolo made a 3 month visit in June - August 2013 to the International Centre for Theoretical Physics (ICTP) in Trieste, Italy, under the Associateship program. Host: Prof Sandro Scandolo.

2013- Recent Visitors

1. The team of Prof Ryo Maezono, Dr Kenta Hongo and Mr Kentaro Hayashi of the Japanese Institute of Science and Advanced Technology (JAIST, Japan) visited our group in March 2013. Dr Kenta Hongo is currently guiding a graduate student (MSc), Carolyne Bakasa, to use the Gaussian code.

2. Professor Mark Casida visited our group in May 2013 under the sponsorship of the French Embassy, Nairobi, and University of Eldoret.

3. George Manyali from University of the Witwatersrand visited our group in August and December 2013. He has participated in the training of scientific mentorship program students.

Local and International Collaborators

1. Local

(a) Robert Gateru – Kenya Methodist University: Area of Experimental Device Physics

(b) Christoper Maghanga – Kabarak University: Area of Solar Energy Energy Materials

(c) Robinson Musembi and Julius Mwabora – University of Nairobi: Area of Solar Energy Materials

2. International

(a) Ryo Maezono and Kenta Hongo – Japan Advanced Institute of Science and Technology (JAIST), Ishikawa, Japan: Area of Computational Materials Science

(b) Daniel Joubert - University of the Witwatersrand (Wits), Johannesburg, South Africa: Area of Computational Materials Science

(c) Sandro Scandolo - International Centre for Theoretical Physics (ICTP), Trieste, Italy: Area of Computational Materials Science

(d) Mark Casida – University of Grenoble, Paris, France: Area of Computational Quantum Chemistry.

(e) Mohammed Hisham – Sultan Qaboos University, Sultanate of Oman: Area of Atomistic Simulations.

Launch of the Scientific Mentorship Program

The first 5 students recruited to participate in the mentorship program were:

1. Elkana Rugut: (Bsc/Physics)

Project Title: Electronic Structure of group 3d Transition Metal Oxides.

2. Sharon Mugangayi: (Bsc/Chemistry and Biochemistry)

Project Title: Modeling of DAVP Class Compounds Targeting HIV Reverse Transcriptase.

3. Alex Mnjama: (Bsc/Chemistry and Biochemistry)

Project Title: In Silico analysis of the promoters of genes involved in Aluminum Tolerance/Resistance in Wheat, Barley, Arabidopsis & Tausch to Identify Regulatory Elements for the Trace.

4. Samson Ngala: (Bsc/Physics)

Project Title: The Prediction of structural, electronic and optical properties of Palladium Hydride (PdH)

5. Eric Buko: (Bsc/Physics)

Project Title: Electronic Structure Studies of the Properties of Ti3O5.

Facilities and Software

1. Sun-Server 52 core cluster funded by the Government of Kenya (National Commission for Science, Technology and Innovation- NACOSTI) and The Academy of Sciences for Developing Nations (TWAS).
2. Linux PC's with secure shell capabilities to connect remotely to sites of our collaborators clusters namely:
    a) Prof. Daniel Joubert, School of Physics, University of the Witwatersrand, South Africa.
    b) Dr Ryo Maezono, Japanese Advanced Institute of Science and Technology (QMC and Quantum Espresso)
3. Computer laboratory with Linux PC's installed with DFT codes – Quantum Espresso, Castep, Open source QMC – Casino, licensed VASP code.
4. Three core i7 PC cluster.

Summary of the Impacts from activities of the Computational Materials Science Group (CMSG)

Some of the noticeable impacts to the University of Eldoret and the country at large have been an increased number of the students taking graduate physics in the country as well as more collaborators between Kenyan researchers and industry than before. Indeed government institutions have inquired into the possibility of partnering with universities to train their staff in key areas relevant to them.

The international community has also shown great interest in collaborating with Kenyan scientists in key research projects of mutual interest.

The Kenya government through its relevant arms has recognized the potential of the CMSG in collaborating towards the development of policies of specialized research centres like the proposed nanotechnology centre as well as the establishment of the national physical sciences research institute (NPSRI) that are expected to impact on the lives of ordinary Kenyans through research of national strategic relevance.

Solid State Communications 179 (2014) 25–28

Contents lists available at ScienceDirect

Solid State Communications

journal homepage: www.elsevier.com/locate/ssc

Ab-initio calculation of formation and migration energies of intrinsic defects in BaF_2

P.W.O. Nyawere [a,b,c,*], S. Scandolo [c,d], N.W. Makau [a], G.O. Amolo [a]

[a] Computational Materials Science Group, Dept of Physics, University of Eldoret, P.O. Box 1125-30100 Eldoret, Kenya
[b] Dept of Computing, Kabarak University, P.O.Box - Private Bag - 20157 Kabarak, Kenya
[c] The Abdus Salam International Centre for Theoretical Physics, Strada Costiera 11-34014 Trieste, Italy
[d] CNR-IOM Democritos National Simulation Center, c/o SISSA - via Bonomea, 265 - 34136, Trieste, Italy

ARTICLE INFO

Article history:
Received 9 August 2013
Received in revised form
30 October 2013
Accepted 11 November 2013
by E.L. Ivchenko
Available online 19 November 2013

Keywords:
A. Barium fluoride
D. Defects
D. Electronic structure

ABSTRACT

We have performed ab-initio calculations of the formation and migration energies of intrinsic defects (interstitials, vacancies and Frenkel defects) in barium fluoride. The calculations were performed within density-functional theory and the generalized-gradient approximation, employing pseudopotentials and a plane-wave basis set. The results agree reasonably well with available experimental data. They are also compatible with calculations and experimental data on calcium fluoride. We found that Frenkel pairs are composed of pairs of charged defects and that their formation energies are 3.44 eV and 1.88 eV for cation and anion, respectively. The lowest barrier for defect migration was found to correspond to the migration of the anion vacancy along the ⟨100⟩ direction (energy barrier of 0.53 eV), which compares well with the experimental value of 0.59 eV. Cation vacancy migration was instead found to require an energy of at least 2.22 eV along the easiest migration path, ⟨100⟩.

1. Introduction

Alkaline-earth fluorides XF_2 (X=Mg,Ca, Sr, Ba) with the cubic fluorite structure constitute an important class of relatively simple ionic crystals with a wide range of applications. CaF_2 [1,15] and BaF_2 have been extensively studied because of their applications in precision vacuum ultraviolet lithography, scintillation detection, as superionic conductors and also in crystalline lens material for precision in VUV optics [2,3]. BaF_2 is one of the fastest scintillators and is also an ideal high-density luminescent material for applications in gamma ray and elementary particle detectors [4]. Just as CaF_2, BaF_2 can be used as an alternative for radiation detection [5]. When particles such as electrons, neutrons or ions with high energy are directed to a target, atoms of the target can be displaced from their original site generating intrinsic defects such as vacancies and interstitials, generally in pairs known as Frenkel defects. A fundamental quantity in the microscopic understanding of the properties and of the suitability of a material for use in radiation detection or as a scintillation detector, is the amount of energy needed to form these defects and the energetic barriers involved in their diffusion. Such properties can also help in the understanding of other properties of the material, such as electrical resistance and mechanical strength [6].

Formation energies for anion defects in BaF_2 can be extracted from ionic conductivity data [2,7]. The experimental data however are limited to anion defects. Moreover, they do not provide information on the microscopic processes at the basis of defect diffusion. Atomistic simulations have been of great help in the interpretation of experimental data in other alkaline-earth fluorides. Earlier studies based on empirical potentials have focused on MgF_2, CaF_2, SrF_2, and BaF_2 [8–10,13,14]. Shi et al. [11,12] have reported on the H and F centers of BaF_2 and CaF_2. The goal of this paper is to determine the formation energies of isolated bulk vacancies, interstitials, and Frenkel defects, as well as the energy barriers for migration of bulk isolated cations and anions in BaF_2, with density-functional theory methods.

We arrange this paper in the following order: we explain the details of the calculation in Section 2, Section 3 discusses the results, and conclusions are in Section 4.

2. Methods

All calculations have been performed in the framework of density functional theory by employing, for the exchange-correlation functional, the generalized gradient approximation of Perdew–Burke–Ernzerhof [16]. Pseudopotentials were taken from the Quantum-Espresso database [17]. For Ba, the pseudopotentials include the semicore states 5s and 5p in the valence. The valence wave functions were expanded in a plane wave basis set truncated at a kinetic energy of 50 Ry (680 eV). At ambient conditions, BaF_2 crystallizes in the cubic fluorite structure ($Fm\bar{3}m, Z=4$) with three

* Corresponding author.
E-mail addresses: pnyawere@yahoo.com, pnyawere@gmail.com (P.W.O. Nyawere), scandolo@ictp.it (S. Scandolo), wanimak@yahoo.com (N.W. Makau), georgeamolo862@gmail.com (G.O. Amolo).

0038-1098/$ - see front matter © 2013 Elsevier Ltd. All rights reserved.
http://dx.doi.org/10.1016/j.ssc.2013.11.017

atoms in the primitive face-centered cubic unit cell and twelve atoms in the conventional simple-cubic cell, with cations at (0, 0, 0), (0, 1/2, 1/2), (1/2, 0, 1/2), and (1/2, 1/2, 0), and anions at $(\pm\frac{1}{4}, \pm\frac{1}{4}, \pm\frac{1}{4})$, in units of the lattice parameter. With our approximations we obtain an equilibrium lattice parameter of 6.10 Å, which compares well with the experimental value of 6.20 Å [18] and with earlier ab-initio calculations (6.05 Å [19] and 6.32 Å [20]). Supercell calculations were performed to study the defect properties and a 96 atom cell was used in all the calculations in this paper. However, a larger unit cell (supercell) may be tested in future which requires increase in computing power. In our case the supercell corresponds to $2\times2\times2$ conventional unit cells and to calculate the formation energy for interstitials, we first calculated the total energy of the perfect crystal (E_c). We then introduced an interstitial in charge state q ($q=0,+2$ for Ba and $q=0,-1$ for F) and calculated the total energy after relaxation, E_i. Thus the interstitial formation energy is given as

$$E_i^f = E_i - E_c - E_a - q(E_{vb}+E_F), \tag{1}$$

where E_a is the energy of a single atom in the vacuum in the case of Ba, and half the energy of a F_2 molecule in vacuum in the case of F, E_{vb} the position of the valence band maximum of the crystal in the calculation with the defect, and E_F is the Fermi energy (chemical potential) of the electrons in the material, measured from the top of the valence band [21]. The correction [21] to the position of the valence band maximum due to difference between the electrostatic potential averaged over the full cell and the electrostatic potential far from the defect was found to be negligible. Because the calculation of E_i corresponds to a charged system, particular care had to be paid to ensure that it was converged with respect to that of the supercell size. To this aim, energies were corrected for spurious interaction between periodic images, at the monopole level [22]. Vacancy formation energies for both cation and anion were calculated by removing one atom of Ba or F, respectively, or their ions, followed by relaxation. The vacancy formation energy E_v^f was defined as

$$E_v^f = E_v - E_c + E_a + q(E_{vb}+E_F), \tag{2}$$

where E_v is the relaxed energy of the crystal containing the vacancy. Notice that the value of the formation energies of interstitials and vacancies depend on the position of the Fermi level and on the choice of the atomic reference, in our case atomic Ba and F atom. The total energy of free F atom was simulated in a large cubic box of dimension 10 Bohr and a value of -48.4171 Ry was obtained to simulate defect energies. Calculated band gap for BaF_2 is 7.2 eV, which is underestimated when compared to the experimental value of $\sim$10 eV. This is a well-known drawback from DFT calculations; where GGA approximations always tend to underestimate the energy band gap [23]. Migration energies were determined as the difference between the total energy of the system with the defect at its stable position before the migration and that with the atom at the saddle point along the migration path. Vacancy migration in the fluorite structure is expected to follow a simple path [24]. Hence the saddle point was obtained by constraining the migration coordinate along a linear path and optimizing the structure at different points along the path.

3. Results and discussion

3.1. Bulk isolated interstitial and vacancy formation energies

For interstitial formation energies, the octahedral site, two bridge sites, and the fourfold hollow site were considered [1]. In agreement with Ref. [1], we found that the octahedral site is preferred, and as such, all calculations reported below refer to the interstitial in the octahedral site. The values of the formation energies are shown in Table 1. The more negative the energy, the easier it is to form such a defect. It is therefore easier to form neutral flourine interstitial than barium interstitial.

Fig. 1 shows the values of the interstitial formation energy for F and F^- as a function of the Fermi energy. In the case of neutral F the formation energy is independent of E_F and is found to be -1.29 eV. For all values of E_F however we find that F^- is more stable than its neutral counterpart. We therefore conclude that the anion interstitial in BaF_2 is negatively charged. The vacancy formation energies calculated upon removing F or F^- are shown in Fig. 2. The formation energy of the neutral vacancy is 9.41 eV. In a large range of values of the E_F (up to about 6 eV), we find that the positively charged F^- vacancy is more stable than its neutral counterpart. Considering that the calculated band gap is 7.2 eV, we conclude that the fluorine vacancy is positively charged except when the bulk is donor-rich.

The results for Ba interstitial and vacancy formation energies are reported in Figs. 3 and 4, respectively. The formation energy of the Ba neutral interstitial is 3.14 eV, but for all values of the Fermi energy within the BaF_2 band gap, the formation energy of the Ba^{2+} interstitial is lower, and therefore the interstitial exists only as a charged species. The same conclusion applies to the Ba vacancy (Fig. 4).

Frenkel defects are defect pairs consisting of an interstitial and of a vacancy produced by the displacement of an atom from a crystal lattice site to a different location in the crystal. In the limit of infinite separation between vacancy and interstitial the formation energy of a Frenkel defect, can be obtained by summing the formation energies of the interstitial and vacancy formation energies. From Figs. 1 and 2, we can argue that fluorine Frenkel defects are always composed of charged pairs, except when the Fermi level is close to the conduction band minimum, in which case the interstitial is charged and the vacancy is neutral. The

Table 1
Interstitial and vacancy formation energies of BaF_2 in eV.

Ion	Interstitial	Vacancy
Ba	3.14	15.64
F	−0.62	8.73
Ba^{2+}	−18.28	21.27
F^-	2.49	−1.06

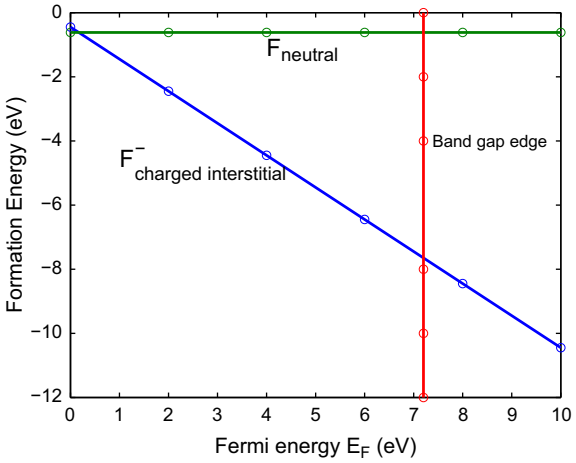

Fig. 1. (Color online) Formation energy as a function of Fermi energy for F and F^- interstitial defects in BaF_2.

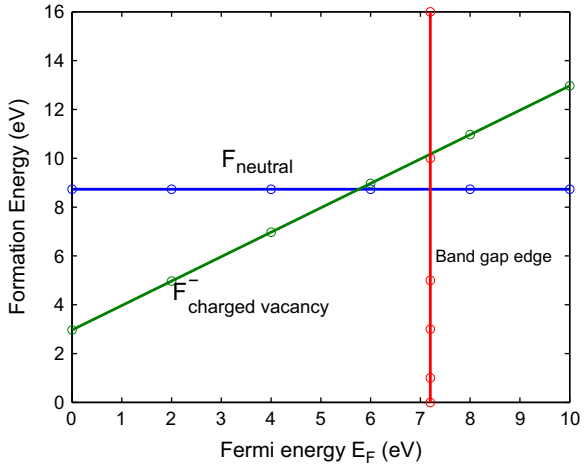

Fig. 2. (Color online) Vacancy formation energies as a function of Fermi energy for F and F^-.

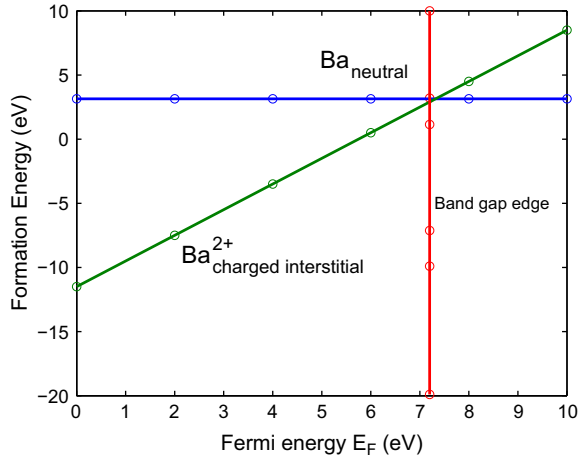

Fig. 3. (Color online) Interstitial formation energies as a function of Fermi energy for Ba and Ba^{2+}.

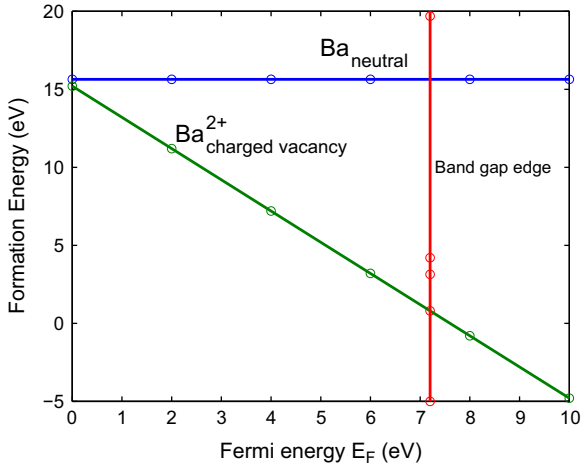

Fig. 4. (Color online) Ba vacancy formation energy as a function of Fermi energy E_F.

formation energy of the F Frenkel defect is 2.33 eV when both defects are charged, and ranges between 2.33 eV and approximately 0.8 eV when the Fermi level is close to the conduction band minimum. From Figs. 3 and 4, we conclude that Barium Frenkel defects are always composed of charged pairs, independent of the Fermi energy, and that their formation energy is 3.90 eV. The values are in good agreement with experimental values extracted from ionic conductivity measurements (1.81 eV for the anion Frenkel defect [2,7]). They are also in line with similar calculations on CaF_2 [15]. The formation energies of the neutral Frenkel defects are also compatible with the calculations of Refs. [1,15].

We also calculated the formation energies of Frenkel defects with the interstitial and the vacancy separated by one or two nearest-neighbor distances. These were carried our with the 96 atoms supercell described in the previous section. We found that when the interstitial is placed in an octahedral site adjacent to the vacancy site, the atomic configuration is unstable and relaxes back to the ideal crystal lattice. On the contrary, when the interstitial is placed in the second-nearest octahedral site from the vacancy site, the atomic configuration is locally stable for the cation and it is still unstable for the anion. The anion becomes locally stable only when it is placed in the third nearest-neighbor interstitial site from the vacancy. The formation energies of the locally stable configurations are 1.4 eV for the anion and 4.1 eV for the cation. If we compare these values with the values obtained for the Frenkel defects at infinite separation, we notice that the cation Frenkel defects find it preferable, once formed, to separate at distances larger than the second-nearest neighbor positions, while anion Frenkel defects find it preferable to reside at finite separation.

Table 2
Vacancy migration energy for cation and anion for BaF_2 in eV.

Direction	Present	Experimental
$V_F\langle 100\rangle$	0.53	0.59 Ref. [2]
$V_F\langle 110\rangle$	1.17	…
$V_F\langle 111\rangle$	1.15	…
$V_{Ba}\langle 100\rangle$	2.22	…

3.1.1. *Bulk isolated vacancy migration energy*

Vacancy migration energies were calculated for the anion diffusion along three crystallographic directions, ⟨100⟩, ⟨110⟩, and ⟨111⟩, respectively (see Table 2). Similar to CaF_2, the lowest barrier for diffusion was found to be along ⟨100⟩ (0.53 eV). This value is in good agreement with experimental data (0.59 eV Ref. [2]).

Regarding the diffusion of cation vacancies, we found that the large size of Ba^{2+} (ionic radius of 1.49 Å), prevents the cation from diffusing easily along ⟨110⟩ and ⟨111⟩. For example, a linear path along the ⟨110⟩ direction brings Ba at a distance of approximately 1.5 Å from nearest fluorine. Therefore we calculated the migration energy only along the crystallographic direction ⟨100⟩, and found it to be 2.22 eV. This is slightly different with respect to recent calculations for CaF_2 where the ⟨100⟩ and ⟨110⟩ directions were found to display very similar energy barriers. This is presumably due to the substantial difference between the ionic radius of Ba^{2+} and Ca^{2+} (1.14 Å).

4. Conclusion

The energies of formation and migration of intrinsic bulk isolated defects in BaF_2 were calculated for both cation and anion using ab-initio methods and the results show good agreement with the available data. Energies are found to be similar to those reported for calcium fluoride. Cation Frenkel defects are most stable at infinite separation while anion Frenkel defects are most stable in the third nearest neighbor. Charged Frenkel defects are more stable than neutral Frenkel defects for both cation and anion and they are locally stable only when the distance between vacancy and interstitial is at least 5 Å and 8 Å for cation and anion respectively.

Acknowledgments

This work has been made possible by the support of the Sandwich Training in Education Program (STEP) of The Abdus Salam International Center for Theoretical Physics. One of the authors (P.W.O.N.) thanks the participants of the African School in Electronic Structure and Materials (ASESMA) for useful discussions.

References

[1] K. Li, H. Xiao, L. Wang, Nucl. Inst. Meth. Phys. B 266 (2008) 2698.
[2] V. Katsika-Tsigourakou, E. Skordas, Cent. Eur. J. Phys. 8 (2010) 900.
[3] H. Ai-Min, G. Chun-Xiao, L. Ming, H. Chun-Yuan, H. Xiao-Wei, Z. Dong-Mei, Y. Cui-Ling, Z. Guang-Tian, L. Yan-Chun, L. Xiao-Dong, Chin. Phys. Lett. 23 (2006) 2917.
[4] H. Jiang, A. Costales, M.A. Blanco, M. Gu, R. Pandey, J.D. Gale, Phys. Rev. B 62 (2000) 803.
[5] Y. Shimizu, M. Minowa, W. Suganuma, Y. Inoue, Phys. Lett. B 633 (2006) 195.
[6] S. Hull, Rep. Progr. Phys. 67 (2004) 1233.
[7] W. Bollmann, Cryst. Res. Technol. 16 (1981) 4014.
[8] D. Chakravorty, J. Phys. Chem. Solids 32 (1971) 1019.
[9] M.J. Gillan, P.W.M. Jacobs, Phys. Rev. B 28 (1983) 759.
[10] S. Keeton, W. Wilson, Phys. Rev. B 7 (1973) 834.
[11] H. Shi, R. Eglitis, R. Jia, Phys. Rev. B 81 (2010) 195101.
[12] H. Shi, R. Eglitis, R. Jia, Solid State Ion. 2011 (2011) 201.
[13] M. Norgett, J. Phys. C: Solid State Phys. 4 (1971) 298.
[14] A. Franklin, J. Phys. Chem. Sol. 29 (1968) 823.
[15] A. Foster, T. Trevethan, A. Shluger, Phys. Rev. Lett. B 80 (2009) 115421.
[16] J.P. Perdew, K. Burke, M. Ernzerhof, Phys. Rev. Lett. 77 (1996) 3865.
[17] P. Giannozzi, J. Phys: Cond. Matt. 21 (2009) 395502.
[18] J.M. Leger, J. Haines, A. Atouf, O. Schulte, S. Hull, Phys. Rev. B 52 (1995) 13247.
[19] K. Schmalzl, Phys. Rev. B 75 (2007) 014306.
[20] H. Jiang, R. Pandey, C. Darrigan, M. Rerat, J. Phys. Cond. Matt. 15 (2003) 709.
[21] C. Van de Walle, J. Neugebauer, J. Appl. Phys. 95 (2004) 3851.
[22] G. Makov, M.C. Payne, Phys. Rev. B 51 (1995) 4014.
[23] Hai Xiao, Jamil Tahir-Keli, et al., J. Phys. Chem. Lett. 2 (2011) 212–217.
[24] K. Sato, T. Yoshiie, T. Ishizaki, Q. Xu, Phys. Rev. B 75 (2007) 094109.

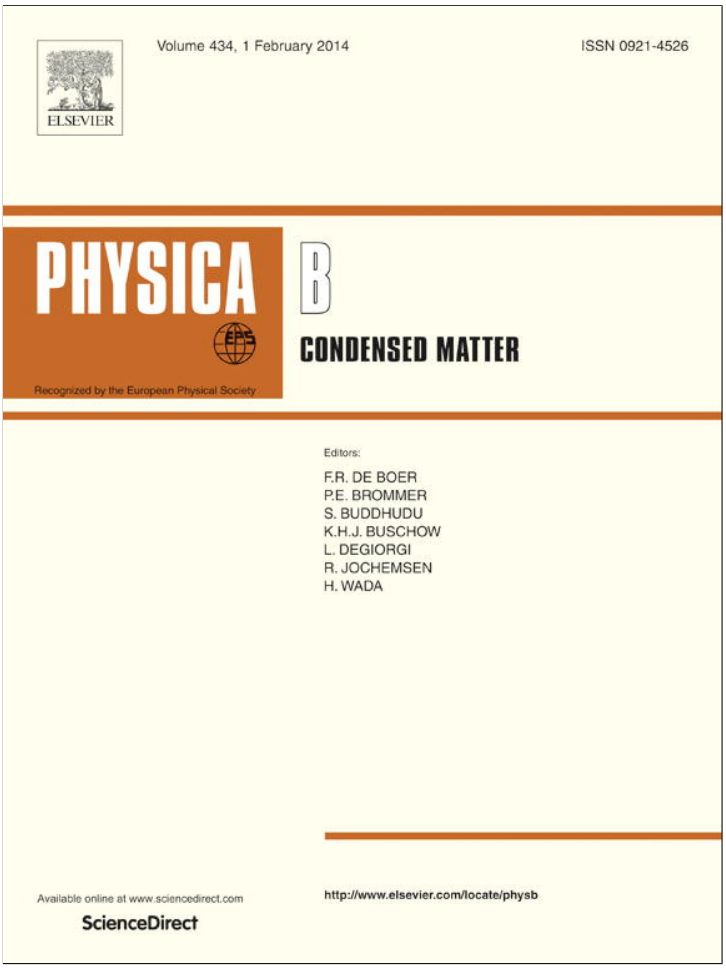

Physica B 434 (2014) 122–128

Contents lists available at ScienceDirect

Physica B

journal homepage: www.elsevier.com/locate/physb

First-principles calculations of the elastic constants of the cubic, orthorhombic and hexagonal phases of BaF_2

P.W.O. Nyawere [a,b,c,*], N.W. Makau [a], G.O. Amolo [a]

[a] Computational Materials Science Group, Department of Physics, University of Eldoret, P.O. Box 1125-30100 Eldoret, Kenya
[b] Department of Computing, Kabarak University, P.O. - Private Bag - 20157 Kabarak, Kenya
[c] The Abdus Salam International Centre for Theoretical Physics, Trieste, Italy

ARTICLE INFO

Article history:
Received 16 May 2013
Received in revised form
24 October 2013
Accepted 27 October 2013
Available online 6 November 2013

Keywords:
Bulk modulus
Anisotropy
Elastic constants

ABSTRACT

All the elastic constants of cubic, orthorhombic and hexagonal phases of BaF_2 have been calculated using first principles methods. We have employed density-functional theory within generalized gradient approximation (GGA) using a plane-wave pseudopotentials method and a plane-wave basis set. The calculated elastic constant values for a cubic phase compare well with recent theoretical and experimental calculations. The bulk modulus derived from the elastic constant calculations of orthorhombic phase of BaF_2 is 94.5 GPa and those of hexagonal phase is 161 GPa. These values are in good agreement with experimental data available. Stability of these phases of BaF_2 is also estimated in different crystallographic directions.

1. Introduction

Elastic constants of solids give important information about their mechanical and dynamical properties. The single crystal elastic constant of solids helps in interpreting seismic wave velocities and their lateral variations. Also, the study of elastic properties of materials helps in the understanding of the chemical bonds and also the cohesion of materials. Elastic properties are also related to the thermal properties according to the Debye theory. This study is a first-principles calculation which has shown success in obtaining elastic properties of other materials [1,2].

BaF_2 is one of the fastest scintillators and is also an ideal high-density luminescent material for applications in gamma ray and elementary particle detectors [3]. In its scintillation property, BaF_2 has a fast core–valence-band transition (cross-luminescence) which represents radiative transition of electrons from valence band which is originally from the 2p states of F^- into the upper core band of the crystal formed by the 5p states of Ba^{2+}. Where necessary, rare earth ions are used as impurities to reduce this self-trapped exciton luminescence [4].

Although various experimental techniques are available for measuring elastic constants, such as ultrasonic wave propagation, neutron scattering and Brillouin scattering, difficulties in preparing suitable specimens for many materials as well as the need to obtain accurate results fast and cheaply make theoretical calculation unavoidable. The alkaline earth fluorides are known to undergo a series of pressure-induced phase transitions to highly coordinated AX_2 structures.

Under ambient conditions, BaF_2 crystallizes in the cubic fluorite structure ($Fm\bar{3}m, Z=4$) with three atoms in the primitive face-centered cubic unit cell and twelve atoms in the conventional simple-cubic cell, with cations at (0, 0, 0), (0, 1/2, 1/2), (1/2, 0, 1/2) and (1/2, 1/2, 0), and anions at $(\pm\frac{1}{4}, \pm\frac{1}{4}, \pm\frac{1}{4})$, in units of the lattice parameter.

BaF_2 undergoes phase transition to the orthorhombic cotunnite-type structure (Pnam, $Z=4$) at about 5 GPa then to a hexagonal phase at pressures between 10 and 15 GPa [5,6]. The orthorhombic phase has twelve atoms in the unit cell; four barium atoms and eight fluorine atoms. The hexagonal phase of BaF_2 ($P6_3mmc(B8_b)$) has six atoms; four fluorine and two barium atoms in the unit cell.

While the elastic constants of cubic phase of BaF_2 have been studied extensively [7], those of low symmetry phases such as tetragonal and hexagonal systems have received little attention. Furthermore, calculation of elastic constants of these low symmetry phases requires more computations and accurate methods for determining total energies. Reduced symmetry also increases the number of independent elastic constants, creating a large number of distortion matrices necessary for calculating these constants. In particular, the cubic phase has only three independent elastic constants while orthorhombic crystals have nine constants. Lastly, the hexagonal symmetry has five elastic constants. The strain

* Corresponding author at: Deparmtent of Computing, Kabarak University, P.O. Private Bag - 20157 Kabarak, Nakuru, Kenya.
Tel.: +25 47 28342054; fax: +254 51 343012.
E-mail addresses: otienop98@yahoo.ca, pnyawere@gmail.com (P.W.O. Nyawere), wanimak@yahoo.com (N.W. Makau), georgeamolo862@gmail.com (G.O. Amolo).

0921-4526/$ - see front matter © 2013 Elsevier B.V. All rights reserved.
http://dx.doi.org/10.1016/j.physb.2013.10.051

needed for calculating the elastic constants of orthorhombic symmetry has been found to lead to the lowest symmetry among the three phases [8].

In Ref. [7], properties of cubic phase of BaF_2 are extensively studied including the elastic constants, phonons and volume–pressure relations. Ref. [8] reported on the structural, electronic and optical properties of BaF_2 in the cubic, orthorhombic and hexagonal phases. Recently, the variation of the independent elastic constants as a function of pressure has been reported [9]. Elastic constants for the cubic, orthorhombic and hexagonal phases of CaF_2 have also been reported [2]. To the best of our knowledge, the elastic constants of hexagonal and orthorhombic phases of BaF_2 have not been investigated. In this paper we study all the elastic constants of the three phases of BaF_2 and mechanical properties using plane wave pseudopotentials (PW-PP) calculations. Our results are compared with theoretical and available experimental data. The rest of this paper is organized in this order: methodology is in Section 2, elastic constants and bulk moduli in Section 3 and Section 4 discusses results while conclusions are in Section 5.

2. Methodology

All calculations have been performed in the framework of density functional theory by employing, for the exchange–correlation functional, the generalized gradient approximation of Perdew–Burke–Ernzerhof [10]. Pseudopotentials were taken from the Quantum-Espresso database [11]. For Ba, the pseudopotentials include the semi-core states 5s and 5p in the valence. The total energy convergence in the iterative solution of the Kohn–Sham equations [12] was set at 2×10^{-8} Ry.

In structural optimization, we used the procedure in Jiang [13] and Schmalz's work [7] and all the calculations were done under ground state conditions. Elastic constants were calculated as the second derivatives of the internal energy with respect to strain tensor (ε) [14]. During structural optimization, the enthalpy was minimized by varying the length of the lattice vectors, while the angles between the lattice vectors and the atomic positions in the unit cell were fixed. The applied strains were isochoric (volume-conserving) which had several important consequences. First was the conservation of the identity of the calculated elastic constants with the strain–stress coefficients, which were appropriate for the calculation of elastic wave velocities but was not important for finite pressure. Second, the total energy depends on the volume much more strongly than the strain and by choosing volume conserving strains we avoided the separation of these two contributions to the total energy. Lastly, the change in the basis set associated with the applied strain was minimized and hence reducing computational uncertainties [7].

Three independent elastic constants for cubic, nine for orthorhombic and five for hexagonal phases of BaF_2 were calculated as mentioned before. Small distortions, δ, between -0.02 and 0.02 at the intervals of 0.002 giving a total of twenty one distortions were considered in all the three phases. Each strain was parametrized by a single variable δ, and the total energy was calculated for each distortion. The calculated total energies were fitted to a polynomial in δ and then equated to the appropriate elastic constant coefficient expression given for each matrix in cubic, orthorhombic and hexagonal phases.

3. Theory

3.1. Cubic phase

The cubic phase has only one lattice parameter a and in this work, a grid of $6\times6\times6$ Monkhorst–Pack [15] k-points was used. The convergence was stopped at a plane wave cut-off energy of $E_{cut}=50$ Ry. Calculation of elastic constants for the cubic phase is less straineous when compared to either the hexagonal or the orthorhombic phases. Our optimized cell volume has lattice dimensions which compare well with other works [7] as noted earlier in Section 1. For a solid under strain, elastic energy is given as follows:

$$\frac{\Delta E}{V}=\frac{1}{2}\sum_{i=1}^{6}\sum_{j=1}^{6}C_{ij}e_ie_j, \tag{1}$$

where V is the undistorted lattice cell volume, ΔE is the energy change from the strain with vector $e=(e_1,e_2,e_3,e_4,e_5,e_6)$ and C is the matrix of the elastic constants [1]. The cubic structure of BaF_2 has its primitive vectors defined as follows:

$$\begin{pmatrix}a_1\\a_2\\a_3\end{pmatrix}=\begin{pmatrix}0&\frac{a}{2}&\frac{a}{2}\\\frac{a}{2}&0&\frac{a}{2}\\\frac{a}{2}&\frac{a}{2}&0\end{pmatrix}, \tag{2}$$

with $\vec{a}$ being the lattice constant. Under strain, the primitive vectors $\vec{a_i}$ $(i=1,2,3)$ are transformed to the new vectors by

$$\begin{pmatrix}a_1'\\a_2'\\a_3'\end{pmatrix}=\begin{pmatrix}a_1\\a_2\\a_3\end{pmatrix}(I+\varepsilon), \tag{3}$$

where ε is the strain tensor which is related to the strain vector e by the following equation:

$$\varepsilon=\begin{pmatrix}e_1&\frac{e_6}{2}&\frac{e_5}{2}\\\frac{e_6}{2}&e_2&\frac{e_4}{2}\\\frac{e_5}{2}&\frac{e_4}{2}&e_3\end{pmatrix}. \tag{4}$$

In order to calculate the elastic constant C_{44}, we applied the triaxial shear strain $e=(0,0,0,\delta,\delta,\delta)$ to the crystal following a similar approach as in Ref. [16]:

$$\frac{\Delta E}{V}=\frac{3}{2}C_{44}\delta^2. \tag{5}$$

The shear modulus C' was then calculated from the volume-conserving orthorhombic strain $e=(\delta,\delta,(1+\delta)^{-2}-1,0,0,0)$ by using the relation given by the following equation:

$$\frac{\Delta E}{V}=6C'\delta^2+O(\delta^3). \tag{6}$$

Lastly, we obtained bulk modulus B from the strain under hydrostatic pressure $e=(\delta,\delta,\delta,0,0,0)$ [1] using the following expression:

$$\frac{\Delta E}{V}=\frac{9}{2}B\delta^2. \tag{7}$$

Using the relations of Eqs. (5)–(7), and knowing that the shear modulus is given as $C'=\frac{1}{2}(C_{11}-C_{12})$, all the three independent elastic constants of the cubic phase of BaF_2 were calculated.

3.2. Orthorhombic phase

The face centered orthorhombic phase of BaF_2 has three lattice parameters $\vec{a}$, $\vec{b}$ and $\vec{c}$. A kinetic energy cut-off of 30 Ry and a k-point grid of $2\times4\times2$ was used in all the calculations reported here. Bravais lattice vector of the orthorhombic phase has a matrix of the form

$$\mathbf{R}=\frac{1}{2}b\begin{pmatrix}0&1&c/b\\a/b&0&c/b\\a/b&1&0\end{pmatrix}. \tag{8}$$

$\mathbf{R}$ can be strained according to the relation $\mathbf{R}'=\mathbf{RD}$, where $\mathbf{R}'$ is the deformed matrix with distorted lattice vectors and $\mathbf{D}$ is the

Table 1
Distortion matrices for the elastic constants for the orthorhombic phase of BaF_2 for the nine elastic constants; C_{11}, C_{22}, C_{33}, C_{44}, C_{55}, C_{66}, C_{12}, C_{13} and C_{23} with the corresponding strain energy per unit volume.

Distortion constant	Distortion matrix	Ratio of energy change to volume
D_1	$\begin{pmatrix} 1+\delta & 0 & 0 \\ 0 & 1 & 0 \\ 0 & 0 & 1 \end{pmatrix}$	$\frac{\Delta E}{V} = \left(\tau_1\delta + \frac{C_{11}}{2}\delta^2\right)$
D_2	$\begin{pmatrix} 1 & 0 & 0 \\ 0 & 1+\delta & 0 \\ 0 & 0 & 1 \end{pmatrix}$	$\frac{\Delta E}{V} = \left(\tau_2\delta + \frac{C_{22}}{2}\delta^2\right)$
D_3	$\begin{pmatrix} 1 & 0 & 0 \\ 0 & 1 & 0 \\ 0 & 0 & 1+\delta \end{pmatrix}$	$\frac{\Delta E}{V} = \left(\tau_3\delta + \frac{C_{33}}{2}\delta^2\right)$
D_4	$\begin{pmatrix} \frac{1}{(1-\delta^2)^{1/3}} & 0 & 0 \\ 0 & \frac{1}{(1-\delta^2)^{1/3}} & \frac{\delta}{(1-\delta^2)^{1/3}} \\ 0 & \frac{\delta}{(1-\delta^2)^{1/3}} & \frac{1}{(1-\delta^2)^{1/3}} \end{pmatrix}$	$\frac{\Delta E}{V} = 2(\tau_4\delta + C_{44}\delta^2)$
D_5	$\begin{pmatrix} \frac{1}{(1-\delta^2)^{1/3}} & 0 & \frac{1}{(1-\delta^2)^{1/3}} \\ 0 & \frac{1}{(1-\delta^2)^{1/3}} & 0 \\ \frac{\delta}{(1-\delta^2)^{1/3}} & 0 & \frac{1}{(1-\delta^2)^{1/3}} \end{pmatrix}$	$\frac{\Delta E}{V} = 2(\tau_5\delta + C_{55}\delta^2)$
D_6	$\begin{pmatrix} \frac{1}{(1-\delta^2)^{1/3}} & \frac{1}{(1-\delta^2)^{1/3}} & 0 \\ \frac{\delta}{(1-\delta^2)^{1/3}} & \frac{1}{(1-\delta^2)^{1/3}} & 0 \\ 0 & 0 & \frac{1}{(1-\delta^2)^{1/3}} \end{pmatrix}$	$\frac{\Delta E}{V} = 2(\tau_6\delta + C_{66}\delta^2)$
D_7	$\begin{pmatrix} \frac{1+\delta}{(1-\delta^2)^{1/3}} & 0 & 0 \\ 0 & \frac{1-\delta}{(1-\delta^2)^{1/3}} & 0 \\ 0 & 0 & \frac{1}{(1-\delta^2)^{1/3}} \end{pmatrix}$	$\frac{\Delta E}{V} = (\tau_1-\tau_2)\delta + \frac{1}{2}(C_{11}+C_{22}-2C_{12}\delta^2)$
D_8	$\begin{pmatrix} \frac{1+\delta}{(1-\delta^2)^{1/3}} & 0 & 0 \\ 0 & \frac{1}{(1-\delta^2)^{1/3}} & 0 \\ 0 & 0 & \frac{1-\delta}{(1-\delta^2)^{1/3}} \end{pmatrix}$	$\frac{\Delta E}{V} = (\tau_1-\tau_3)\delta + \frac{1}{2}(C_{11}+C_{33}-2C_{13})\delta^2$
D_9	$\begin{pmatrix} \frac{1}{(1-\delta^2)^{1/3}} & 0 & 0 \\ 0 & \frac{1+\delta}{(1+\delta^2)^{1/3}} & 0 \\ 0 & 0 & \frac{1-\delta}{(1-\delta^2)^{1/3}} \end{pmatrix}$	$\frac{\Delta E}{V} = (\tau_2-\tau_3)\delta + \frac{1}{2}(C_{22}+C_{33}-2C_{23})\delta^2$

symmetric distortion matrix, which contains the strain components. Since we have nine independent elastic constants, we need nine different strains to determine them. The nine distortion matrices used in the present calculations are described in the distortion matrices D_1–D_9 given in Table 1 with the corresponding change in energy to volume ratio. The nature of distortions that these matrices create has been described by Ravindran [8] and is given in Tables 1 and 2. Bulk modulus for the orthorhombic phase $B_{ortho.}$ derived from the elastic constants is given as follows:

$$B_{ortho.} = \frac{\Lambda}{(1+\gamma+\sigma)^2} \tag{9}$$

where

$$\Lambda = C_{11} + 2C_{12}\gamma + C_{22}\gamma^2 + 2C_{13}\sigma + C_{33}\sigma^2 + 2C_{33}\gamma\sigma \tag{10}$$

$$\sigma = \frac{(C_{11}-C_{12})(C_{33}-C_{13}) - (C_{23}-C_{13})(C_{11}-C_{13})}{(C_{33}-C_{13})(C_{22}-C_{12}) - (C_{13}-C_{23})(C_{12}-C_{23})} \tag{11}$$

$$\gamma = \frac{(C_{22}-C_{12})(C_{11}-C_{13}) - (C_{11}-C_{12})(C_{23}-C_{12})}{(C_{22}-C_{12})(C_{33}-C_{13}) - (C_{12}-C_{23})(C_{13}-C_{23})} \tag{12}$$

3.3. Hexagonal phase

The same approach employed for the orthorhombic phase [17] was used for the hexagonal phase only that the hexagonal phase of BaF_2 has two lattice parameters a and c with Bravais lattice vectors in matrix form

$$\mathbf{R} = \begin{pmatrix} \frac{\sqrt{3}}{2}a & -\frac{1}{2}a & 0 \\ -\frac{\sqrt{3}}{2}a & \frac{1}{2}a & 0 \\ 0 & 0 & \frac{c}{a} \end{pmatrix}. \tag{13}$$

The k-point grid used in this case was $6\times6\times3$ with a cut-off energy of 35 Ry. Again $\mathbf{R}$ can be strained according to the relation $\mathbf{R}' = \mathbf{RD}$ where $\mathbf{R}'$ is the deformed matrix with distorted lattice

Table 2
Distortion matrices for the elastic constants for the hexagonal phase of BaF_2.

Distortion constant	Distortion matrix	Ratio of energy change to volume
D_{10}	$\begin{pmatrix} 1+\delta & 0 & 0 \\ 0 & 1+\delta & 0 \\ 0 & 0 & 1+\delta \end{pmatrix}$	$\frac{\Delta E}{V} = (\tau_1+\tau_2+\tau_3)\delta + \frac{1}{2}(2C_{11}+2C_{12}+4C_{13}+C_{33})\delta^2$
D_{11}	$\begin{pmatrix} (1+\delta)^{-1/3} & 0 & 0 \\ 0 & (1+\delta)^{-1/3} & 0 \\ 0 & 0 & (1+\delta)^{-2/3} \end{pmatrix}$	$\frac{\Delta E}{V} = (\tau_1+\tau_2+\tau_3)\delta + \frac{1}{9}(C_{11}+C_{12}-4C_{13}+2C_{33})\delta^2$
D_{12}	$\begin{pmatrix} \frac{1+\delta}{(1-\delta^2)^{1/3}} & 0 & 0 \\ 0 & \frac{1-\delta}{(1-\delta^2)^{1/3}} & 0 \\ 0 & 0 & \frac{1}{(1-\delta^2)^{1/3}} \end{pmatrix}$	$\frac{\Delta E}{V} = (\tau_1-\tau_2)\delta + (C_{11}-C_{12})\delta^2$
D_{13}	$\begin{pmatrix} \frac{1}{(1-\delta^2)^{1/3}} & 0 & \frac{\delta}{(1-\delta^2)^{1/3}} \\ 0 & \frac{1}{(1-\delta^2)^{1/3}} & 0 \\ \frac{\delta}{(1-\delta^2)^{1/3}} & 0 & \frac{1}{(1-\delta^2)^{1/3}} \end{pmatrix}$	$\frac{\Delta E}{V} = \tau_5\delta + (2C_{55})\delta^2$
D_{14}	$\begin{pmatrix} 1 & 0 & 0 \\ 0 & 1 & 0 \\ 0 & 0 & 1+\delta \end{pmatrix}$	$\frac{\Delta E}{V} = \tau_3\delta + \left(\frac{C_{33}}{2}\right)\delta^2$

vectors and **D** is the symmetric distortion matrix, which contains the strain components. Since we have five independent elastic constants, five different strains were used to determine them. The distortion matrices D_{10}–D_{14} shown in Table 2 were applied to deform the crystal and obtain the relevant relations necessary to calculate the required elastic constants. Bulk modulus for the relaxed hexagonal phase $B_{hexa.}$ is given as follows:

$$B_{hexa.} = \frac{2(C_{11}+C_{12})+4C_{13}+C_{33}}{9} \tag{14}$$

3.4. Stability of the phases

Zener anisotropy A is an indicator of the degree of anisotropy in the solid structure compared to the isotropic material [1]. For the cubic phase, the Zener anisotropy is given as follows:

$$A = \frac{2C_{44}}{C_{11}-C_{12}}. \tag{15}$$

When coordinates of ions are optimized, internal strain is released and from those optimized coordinates, the Kleinman internal-strain parameter ξ is given as [18]

$$\xi = \frac{C_{11}+8C_{12}}{7C_{11}+2C_{12}}. \tag{16}$$

The macroscopic elastic constants, bulk modulus B and elastic shear constant given as $C' = (C_{11}-C_{12})/2$ are related to bond-bending force constant β and bond-stretching force constant α [14] by the following equations:

$$3B = \frac{\sqrt{3}}{4d}(3\alpha+\beta) - 0.355SC_o, \tag{17}$$

and

$$C' = \frac{\sqrt{3}}{2d}\beta - 0.053SC_o, \tag{18}$$

where SC_o is the Coulomb contribution and d is the bond length, a parameter that needs to be calculated so as to determine these properties. If we neglect this latter quantity, the bond-stretching force constant α and bond-bending force constant β can be obtained from

$$\beta = \frac{2d}{\sqrt{3}}\frac{C_{11}-C_{12}}{2} \tag{19}$$

and

$$\alpha = \frac{4d}{\sqrt{3}}B - \frac{1}{3}\beta \tag{20}$$

From our cubic structure, d between dissimilar ions is approximated as 2.642 Å.

Table 7 lists data for cohesive energy ΔE_{Ba-F} for the cubic phase of BaF_2, the Zener anisotropy factor, A, and Kleinman internal-strain parameter ξ for the same phase. A and ξ are calculated from the elastic parameters of their respective cubic phases. The difference in cohesive energy ΔE_{Ba-F} is given for a pair of dissimilar atoms.

The Zener anisotropy factors in the orthorhombic phase are three; firstly, A_1 which is the shear anisotropic factor for the {1 0 0} shear planes between the ⟨0 1 1⟩ and ⟨0 1 0⟩ directions. Secondly, A_2 which is the shear factor in the {0 1 0} shear planes between ⟨1 0 1⟩ and ⟨0 0 1⟩ directions. Lastly, for the {0 0 1} direction the shear plane between ⟨1 1 0⟩ and ⟨0 1 0⟩ is given as A_3 [8]. These factors are given as follows:

$$A_1 = \frac{4C_{44}}{C_{11}+C_{33}-2C_{13}} \tag{21}$$

$$A_2 = \frac{4C_{55}}{C_{22}+C_{33}-2C_{23}} \tag{22}$$

and

$$A_3 = \frac{4C_{66}}{C_{11}+C_{22}-2C_{12}}. \tag{23}$$

The hexagonal phase has anisotropy A_1 and A_2 which are given as follows:

$$A_1 = \frac{1}{2C_{44}} + \frac{C_{33}+2C_{13}}{2(2C_{13}^2-C_{33})(C_{11}+C_{12})} - \frac{1}{2(C_{11}-C_{12})} \tag{24}$$

$$A_2 = \frac{1}{2C_{44}} + \frac{C_{11}+C_{12}+C_{13}}{2(C_{13}^2 - C_{33})(C_{11}+C_{12})}. \quad (25)$$

4. Results

4.1. Structural optimization

Table 3 shows the properties obtained for the structural optimization of the cubic, orthorhombic and hexagonal phases of BaF_2.

The computed structural properties show good agreement with both theoretical and experimental calculations. The cubic phase has the least deviation from experimental data showing a lattice constant contraction of about 3.1%. The calculated cell parameters for the orthorhombic unit cell compare well with the corresponding experimental values with a deviation of about 7% of lattice constant a. However other values such as b/a and c/a show good agreement between theory and experiment. The deviation from the experimental lattice constant for the hexagonal phase is 4.5% and about 14% for b/a.

Table 3
Structural optimization results of the cubic, orthorhombic and hexagonal phases of BaF_2 at zero pressure.

Cubic (C1)	a (Å)	b/a	c/a	Ref.
Quantum espresso (GGA)	6.01			Present
ABINIT (LDA)	6.05			Ref. [7]
CRYSTAL (GGA)	6.32			Ref. [13]
Expt. (300 K)	6.20			Ref. [5]
Orthorhombic (C23)				
Quantum espresso (GGA)	6.692	1.158	0.598	Present
CRYSTAL (GGA)	6.871	1.174	0.608	Ref. [13]
Expt. (300 K)	6.159	1.275	0.646	Ref. [5]
Hexagonal ($B8_b$)				
Quantum espresso (GGA)	4.269	1.4894	–	Present
CRYSTAL (GGA)	4.501	1.373	–	Ref. [13]
Expt. (300 K)	5.516	1.297	–	Ref. [5]

Table 4
Elastic constants of the cubic phase of BaF_2 (GPa). The results are compared with other theoretical results and experimental data.

Method	C_{11}	C_{12}	C_{44}	Ref.
Quantum espresso	88.2	34.3	19.6	Present
ABINIT	112.40	64.89	28.76	[7]
Expt. (300 K)	91.22	41.48	25.51	Ref. [7] and references therein
Expt. (0 K)	98.10	44.81	25.44	Ref. [7] and references therein

4.2. Elastic constants

Table 4 shows the elastic constants of the cubic phase of BaF_2 calculated using different theoretical methods and results compared with experimental data. Although the cubic elastic constants of BaF_2 have been studied extensively, it was still necessary to calculate these in the current work so as to confirm them using a different approach as well as validating the calculated elastic constants for other phases of BaF_2 where experimental results were unavailable. It is here shown that our calculated elastic constants for the cubic phase compare quite well with other works. For example, compared to ABINIT calculations, our errors were lower. In particular, error for C_{11} in our case was 3.2% and about 23% for ABINIT compared to experimental value. For C_{12} our error was 17% and 56% for ABINIT. Our C_{44} had the largest error of 23% compared with 13% for ABINIT. These errors are attributed to the fact that our use of GGA pseudopotentials underestimates the elastic constants while the use of LDA in ABINIT overestimates the elastic constants.

Figs. 1–3 show the plots used to obtain parameters needed in the computation of the elastic constants. These are associated to the distortion constants D shown in Tables 1 and 2. In particular Fig. 1 is used for the cubic phase while Figs. 2 and 3 are used for orthorhombic and hexagonal phases of BaF_2, respectively. Each figure shows the parabolic shape predicted by their respective equations as shown in Section 3.

Table 5 shows elastic constants for the orthorhombic phase of BaF_2. In comparison with cubic and orthorhombic phases of BaF_2, the hexagonal phase has the largest C_{11} and C_{12} values (Table 6). This suggests that the hexagonal phase of BaF_2 is the most stiff phase among the three phases as predicted by Jiang et al. [13]. The bulk moduli of the orthorhombic and hexagonal phases are calculated from the derived values of the elastic constants as discussed in Ravindran et al. [8,17] and the results are given in Table 8.

The shear anisotropic factors for the orthorhombic and hexagonal phases of BaF_2 are shown in Table 8. An isotropic material has the factors A_1, A_2 and A_3 equal to one while any other value less or greater than one indicates the degree of anisotropy. From Table 8, the orthorhombic and hexagonal phases of BaF_2 are

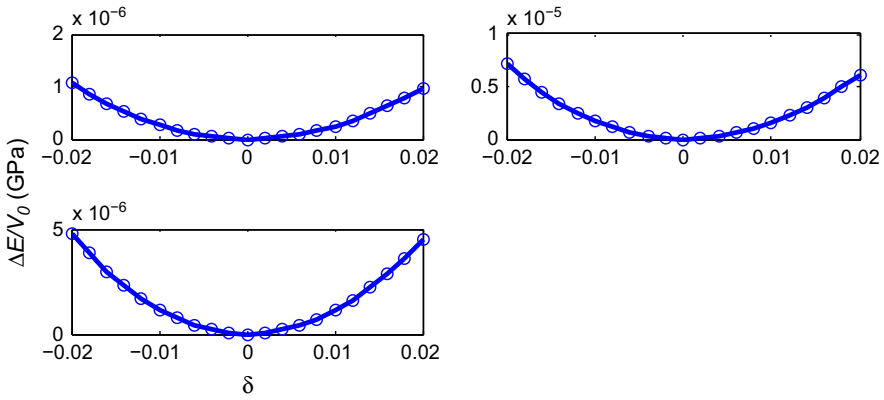

Fig. 1. Variation of $\Delta E/V_0$ with δ for calculating elastic constants of the cubic phase of BaF_2. (a) Fit for C_{44}, (b) corresponds to shear modulus C' and (c) fit for bulk modulus B.

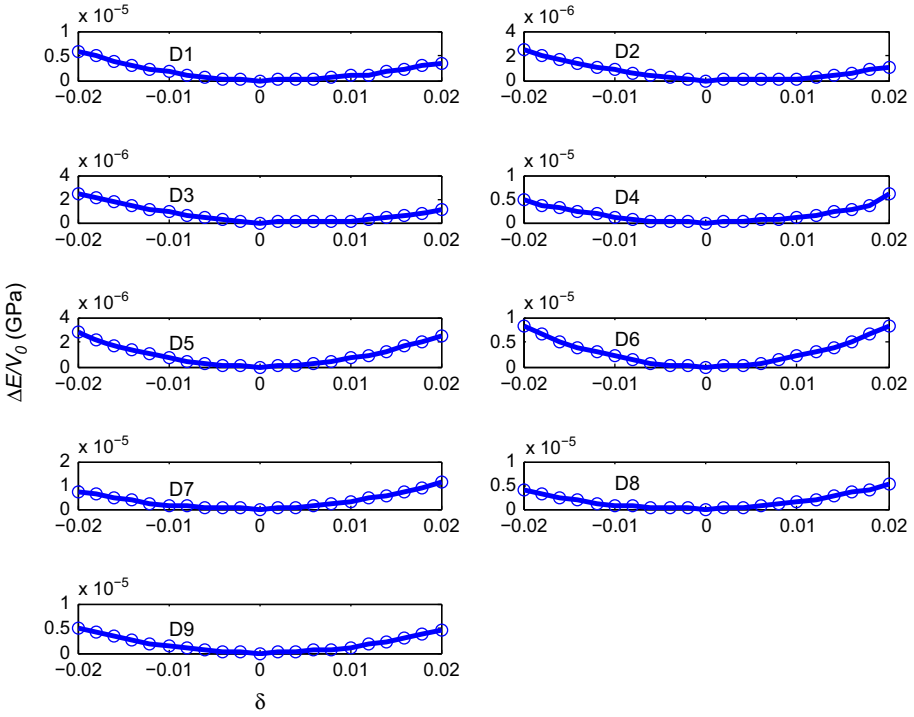

Fig. 2. Changes in the pressure ($\Delta E/V_0$ as a function of strain δ) for the orthorhombic phase of BaF_2. The dots represent the calculated values and the solid lines are the polynomial fit. The $D1$–$D9$ correspond to the distortion matrices given in Section 3.2.

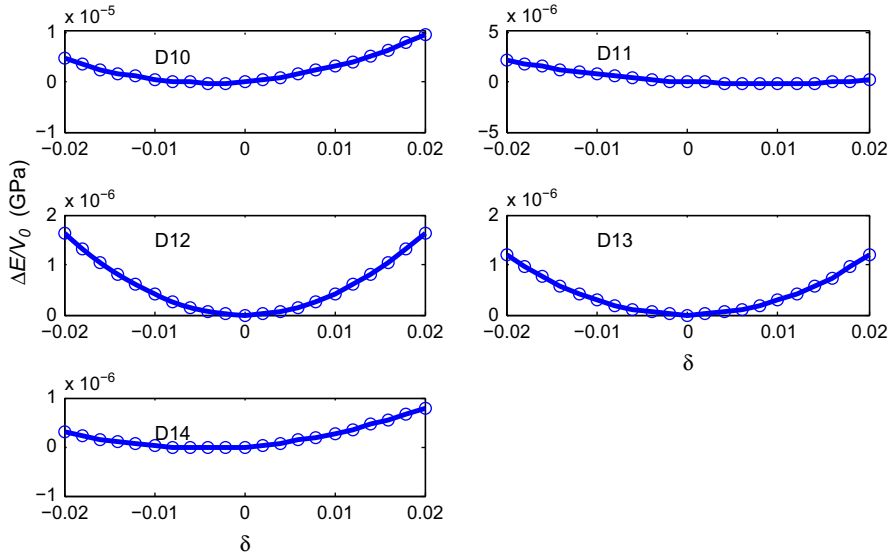

Fig. 3. Variation of $\Delta E/V_0$ versus δ for the calculation of elastic constants of the hexagonal phase of BaF_2. $D1$–$D3$ and $D10$ and $D11$ are the distortions used to calculate the plots. The dots represent the calculated values and the solid lines are the polynomial fits.

Table 5
Elastic constants for the orthorhombic phase of BaF_2 in GPa.

Elastic constant	C_{11}	C_{22}	C_{33}	C_{44}	C_{55}	C_{66}	C_{12}	C_{13}	C_{23}
Quantum espresso	275.5	346	126	91.7	47.2	147.5	32	39	60
Expt.	–	–	–	–	–	–	–	–	–

Table 6
Elastic constants for hexagonal phase of BaF_2 in GPa.

Elastic constant	C_{11}	C_{12}	C_{33}	C_{55}	C_{13}
Quantum espresso	460	399	41	21.7	138.5
Expt.	–	–	–	–	–

anisotropic though the degree of anisotropy varies with the phase and the direction of study. Given that A_2 is greater than A_1 in the hexagonal phase means that contraction is easiest in any direction normal to the hexagonal axis [19]. In addition, the hexagonal phase is anisotropic in all directions for BaF_2 according to values shown in Table 8.

Table 7
Stability properties of cubic phase of BaF_2.

Phase	A	ξ	ΔE_{Ba-F} (eV)	Bulk modulus B (GPa)
Cubic (present)	0.727	0.56	24.87	535
Cubic (ABINIT)	1.21	0.732	–	–

Table 8
Stability properties of orthorhombic and hexagonal phases of BaF_2.

Phase	A_1	A_2	A_3	Bulk modulus B (GPa)
Orthorhombic	1.13	0.54	0.86	94.5
Hexagonal	0.015	0.023		161

5. Conclusion

In this work, the elastic constants of the three phases of BaF_2 have been calculated using first-principles plane wave pseudopotentials. The elastic constants for cubic phase are in good agreement with both experimental and other theoretical works. All the elastic constants of orthorhombic and hexagonal phases of BaF_2 have been calculated for the first time. These values are used to calculate the bulk modulus of these phases and a good agreement is established with other calculations. Stability of these phases shows that the hexagonal phase has the least anisotropy in all directions indicating least stability. In fact, the anisotropy of this hexagonal phase is so low that it is not near those of cubic and orthorhombic phases. This agrees well with the experimental findings that at about 17 GPa, BaF_2 is existing only in the hexagonal phase.

Acknowledgments

This work has been supported by the Sandwich Training Educational Program (STEP) of the International Center for Theoretical Physics, Trieste, Italy. Useful discussions with Kris Delaney of University of California Santa Babara (UCSB) are highly appreciated.

References

[1] S. Wang, J. Phys.Condens. Matter 15 (2003) 5307.
[2] H. Shi, W. Luo, B. Johansson, R. Ahujia, J. Phys.: Condens. Matter 21 (2009) 415501.
[3] H. Jiang, A. Costales, M. Blanco, M. Gu, R. Pandey, J. Gale, Phys. Rev. B 62 (2000) 803.
[4] B. Sobolev, A. Golubev, P. Herrero, Crystallogr. Rep. 48 (2003) 141.
[5] J. Leger, J. Haines, A. Atouf, O. Schuttle, S. Hull, Phys. Rev. B 52 (1995) 13247.
[6] J. Leger, J. Haines, A. Atouf, Phys. Rev. B 51 (1995) 3902.
[7] K. Schmalzl, Phys. Rev. B 75 (2007) 14306.
[8] P. Ravindran, L. Fast, A. Korzhavyi, B. Johansson, J. Appl. Phys. 84 (1998) 4891.
[9] X. Yang, A. Hao, X. Wang, X. Liu, Y. Zhu, Comput. Mater. Sci. 49 (2010) 530.
[10] J. Perdew, K. Burke, M. Ernzerhof, Phys. Rev. Lett. 77 (1996) 3865.
[11] P. Giannozzi, et al., J. Phys.: Condens. Matter 21 (2009) 395502. (19pp).
[12] W. Kohn, L. Sham, Phys. Rev. 140 (1965) A1133.
[13] H. Jiang, R. Pandey, C. Darrigan, M. Rerat, J. Phys.: Condens. Matter 15 (2003) 709.
[14] R. Martin, Phys. Rev. B 6 (1972) 4546.
[15] H. Monkhorst, Phys. Rev. B 20 (1976) 1504.
[16] Y. Wu, W. Hu, S. Han, Phys. B: Phys. Condens. Matter 403 (2008) 3792.
[17] P. Ravindran, P. Vajeeston, R. Vidya, A. Kjekshus, H. Fjellvag, Phys. Lett. A 64 (2001) 224509.
[18] A. Zaoui, M. Ferhat, M. Certier, H. Aourang, B. Khelifa, Phys. Lett. A 228 (1997) 378.
[19] I. Ipatova, L. Lifchits, A. Mastov, 11th International Symposium on Nanophysics and Technology, vol. 1, 2003, p. 1.